IOP Conf. Series: Materials Science and Engineering **400** (2018) 042055 doi:10.1088/1757-899X/400/4/042055

Numerical Simulation of Elastic Bilayered Contact. Part II – Stress State Analysis

S Spinu[1,2] and D Cerlinca[1,2]
[1]Department of Mechanics and Technologies, Stefan cel Mare University of Suceava, 13th University Street, 720229, Romania
[2]Integrated Center for Research, Development and Innovation in Advanced Materials, Nanotechnologies, and Distributed Systems for Fabrication and Control (MANSiD), Stefan cel Mare University, Suceava, Romania

E-mail: sergiu.spinu@fim.usv.ro

Abstract. In a tribological system containing protective coatings, the knowledge of stresses generated in both the hard layer and the substrate are essential to the design of the tribological elements. The stress field due to the contact load is required to assess the coating performance and to guide the coating design. Rough contact analyses can only be performed numerically, but conventional techniques applied to layered solids may lead to very time-consuming simulations. The semi-analytical method for the analyses of contact stresses in a bilayered medium advanced in the companion paper is enhanced and applied to stress analyses in the layered body. The main difficulty in applying FFT-based spectral analysis to the study of subsurface stresses consists in the treatment of the frequency response function (FRF) at the origin of the frequency domain, where the FRF may be singular. As the FRF is integrable in the neighbourhood of the origin, the discrete sample corresponding to the patch centred in origin is substituted by the average value over the latter patch. The conditions of stress continuity at the interface between the protective layer and the substrate are verified. The influence of both coating thickness and dissimilarity in the elastic properties between the coating and the substrate, on the intensity of the maximum von Mises equivalent stress, is assessed. The numerical examples prove the method ability to tackle contact scenarios involving protective coatings and to assist the design of competent tribological elements.

1. Introduction

The competent design of machine elements may involve protective coatings or layers that provide high wear resistance and long fatigue life. The knowledge of stresses arising in the coated bodies under contact load is of paramount importance for predicting the performance and reliability of the coated system.

The analysis of elastic contacts involving layered solids requires the use of numerical methods, especially when realistic and technologically significant three-dimensional configurations are considered, involving contacting surfaces with complex shapes, such as in rough contact problems. In the latter case, meshes with very large numbers of elements lead to high computational costs that are unsuitable for practical purposes.

The use of integral transforms [1-4] reduces the number of spatial dimensions in the numerical treatment of layered solids. The discrete Fourier transform, which can be efficiently evaluated by

means of the fast Fourier transform (FFT) algorithm, further reduces the computational cost. Ju and Farris [5] pioneered the application of FFT to contact mechanics. They calculated stresses generated by a complete contact of 2D rough surfaces and solved a partial contact problem for a pair of smooth 2D surfaces. Nogi and Kato [6] later combined the FFT with the conjugate gradient method for solving linear systems of equations, resulting in a fast numerical technique for rough contact problems involving both homogenous and layered solids. The main issue with the FFT-based methods is the implicit problem periodization, which introduces an error referred to as the periodicity error. Different authors proposed techniques to circumvent this error: Ju and Farris [5] employed a domain-extension, Ai and Sawamiphakdi [7] decomposed the contact traction into a smooth and a zero-mean fluctuating part, whereas Polonsky and Keer [8] constructed a hybrid algorithm by adding a special correction term computed with a multi-level multi-summation technique. An important breakthrough was achieved by these authors [9] with the DCFFT technique, combining the discrete convolution theorem with the processes of zero padding and wrap-around order. The DCFFT method avoids the periodicity error associated with FFT at a cost of only doubling, in every direction, the computational domain of the contact problem. Liu and Wang [10] later applied the DCFFT technique to the study of contact stress fields caused by surface tractions, in which the shear tractions were assumed proportional to pressure. Wang et al. [11] investigated the partial slip contact of coated bodies, by combining the DCFFT with a numerical solution to the Cattaneo-Mindlin problem. The problem was recently revisited by Yu et al. [12], who derived the analytical frequency response functions (FRFs) for stresses in multilayered materials in a recurrence format.

The goal of this paper is to extend the algorithm for displacement computation in a layered medium proposed in the companion paper, and to perform a stress state analysis in the spherical contact involving a bilayered half-space. To this end, the matter of the singularity of the FRF at the origin of the frequency domain must be addressed.

2. Stress field in a layered elastic half-space

A bilayered material with a single layer coating on top of a half-space is considered. Both the layer and the half-space are assumed linear elastic, homogenous and isotropic, with the Young's modulus E_i and the Poisson's ratio ν_i, where $i=1$ refers to the layer and $i=2$ to the half-space. The layer thickness is denoted by h. The interface is perfectly bonded without slip. The problem is reported to Cartezian coordinates x, y and z_i, $i=1,2$, with the origin of the z-axis for each layer located on its top. The stresses and displacements are consequently expressed as functions of x, y and z_1 in the layer, and of x, y and z_2 in the half-space. In order to solve the quasi-static normal contact problem, the solution for arbitrary boundary loading $p(x,y)$ is required. On the surface (i.e., at $z_1=0$), the normal and tangential tractions must obey the boundary conditions corresponding to a frictionless contact problem under normal load, (equations (1, 2):

$$\sigma_{zz}^{(1)}(x,y,0) = -p(x,y)\,; \tag{1}$$

$$\sigma_{zx}^{(1)}(x,y,0) = 0\,; \quad \sigma_{zy}^{(1)}(x,y,0) = 0\,, \tag{2}$$

whereas the continuity condition of tractions and displacements at the interface yields, equations (2-6):

$$\sigma_{zz}^{(1)}(x,y,h) = \sigma_{zz}^{(2)}(x,y,0)\,; \tag{3}$$

$$\sigma_{zx}^{(1)}(x,y,h) = \sigma_{zx}^{(2)}(x,y,0)\,; \tag{4}$$

$$\sigma_{zy}^{(1)}(x,y,h) = \sigma_{zy}^{(2)}(x,y,0)\,; \tag{5}$$

$$u_i^{(1)}(x,y,h) = u_i^{(2)}(x,y,0),\ i = x,y,z. \tag{6}$$

The superscripts (1) and (2) refer to the layer and the half-space, respectively. Additional constraints yield from the condition that, at infinity in the half-space (i.e., for large z_2), the solution must remain bounded, equations (7, 8):

$$u_i^{(2)}(x,y,\infty) = 0,\ i = x,y,z\,; \tag{7}$$

$$\sigma_{ij}^{(2)}(x,y,\infty) = 0,\ i,j = x,y,z\,. \tag{8}$$

The stresses and displacements in the layered system were expressed in the literature [6,10,12] as functions of the Papkovich-Neuber potentials, by taking their double Fourier transform with respect to the x and y, and by imposing the conditions (1) - (8). The closed form expression of the six tensor components derived in the Fourier transform domain (i.e., the frequency response functions), for both the layer and the substrate, are given in Appendix.

3. Algorithm description

The semi-analytical method employed in the companion paper for displacement calculation is extended to allow for the computation of stresses in the layered elastic half-space. Stresses induced by a pressure distribution $p(x,y,0)$ can be expressed as convolution products along the tangential directions x and y, (equation (9):

$$\sigma_{ij}(x,y,z_k) = \int_{-\infty}^{+\infty}\int_{-\infty}^{+\infty} p(x,y,0)\,g_{ij}(\xi - x, \zeta - y, z_k)\,d\xi\,d\zeta\ ,\ i,j = x,y,z,\quad k = 1,2\,, \tag{9}$$

in which g_{ij} denotes the Green's functions, i.e. the analytical relationship between the elastic response (stress) and the Dirac excitation (a unit point force compressing the surface). The Green's functions is only available in the frequency domain as the FRF, therefore the stress analysis is performed by the same technique used for displacement computation in the companion paper. The contact problem involving layered materials was solved by replacing the continuous pressure distribution with a discrete set of pressure elements, while the boundary conditions were imposed at a discrete number of matching points. The displacement computation was performed for the matching points in the frequency domain with the aid of the discrete convolution theorem. Capitalizing on the fact that stresses can also be expressed as the convolution product between the surface tractions and the Green's functions for stresses, which are known in the frequency domain only, the same technique can be applied for stress calculation. An additional difficulty arises as the displacement computed with the method proposed in the companion paper is undetermined to the extent of an arbitrary constant (i.e. only relative displacements of the surface points are known). Whereas this undetermination does not obstruct the resolution of the contact problem, it is clearly that the stress analysis in the elastic body requires absolute stress values in order to predict plastic yield and/or crack nucleation. The source of the undetermination is the discrete value of the FRF corresponding to origin, which cannot be computed from the closed-form expressions as the FRFs as the latters are singular in that point.

Nogi and Kato [6] indicated that, although the FRFs for displacement and stresses may be singular in origin, they are integrable everywhere. Consequently, the integrals of the FRFs over a domain centred in origin may be computed numerically. The method applied in this paper follows the suggestion given in [6], to replace the missing discrete sample with the average value of the FRF over the element centred in origin.

Let $\tilde{g}$ denote any of the FRFs expressing the stresses induced in a layered elastic half-space. Surface discretization in the time / space domain is performed with a data interval of Δ_x and Δ_y along directions of x and y, respectively, leading to a series with $N_x \times N_y$ terms. In the frequency domain,

discretization implies that $\tilde{g}$ is assumed constant in each elementary spectral element of sides lengths $2\pi/(N_x\Delta_x)$ and $2\pi/(N_y\Delta_y)$, and equal to the value of $\tilde{g}$ computed in the centre of the element. By exception, for the spectral element centred in origin of the frequency domain, the representative value is computed as follows, (equation (10):

$$\hat{g}(0,0)=\frac{\int_{-\frac{\pi}{N_y\Delta_y}}^{\frac{\pi}{N_y\Delta_y}}\int_{-\frac{\pi}{N_x\Delta_x}}^{\frac{\pi}{N_x\Delta_x}}\tilde{g}(x,y)dxdy}{\frac{2\pi}{N_x\Delta_x}\frac{2\pi}{N_y\Delta_y}}, \tag{10}$$

where the integral is calculated numerically. In this manner, the undetermination is lifted and the stress field inside the layered material can be computed in layers of constant depth $z_i =$ constant. For every layer, each of the six stress tensor components is expressed as a convolution product that can be efficiently computed in the frequency domain. In this manner, stresses are obtained in the same manner as displacement, in a reunion of points that mirrors in depth the surface representative points used in the resolution of the contact problem.

Whereas the grid should be uniform along the convolution directions, as required by the DCFFT technique, this is not a constraint for depth discretization. Consequently, the grid along the z-axis can be refined in regions where important stress gradients are anticipated or where stresses are of particular interest.

4. Numerical simulations and results

The proposed numerical simulation technique can compute the stress state for arbitrary boundary loading. However, for comparison purposes, the present stress analysis is performed in the frictionless, quasi-static contact of a rigid sphere pressed against a bilayered halfspace. The elastic medium consists in a semi-infinite substrate of elastic parameters E_1, ν_1, and a perfectly bonded elastically dissimilar layer of parameters E_2, ν_2. The Hertz contact for the homogenous half-space (i.e., when $E_1 = E_2$ and $\nu_1 = \nu_2$) is considered as reference. To this end, the following parameters are kept constant during the simulations: the normal load, the contact geometry, the Young modulus of the substrate E_2, the Poisson's ratios for both the coating and the substrate ($\nu_1 = \nu_2 = 0.3$), whereas the Young modulus of the coating E_1 and the coating thickness h are varied. The Hertz contact model yields the contact radius a_H and the central maximum pressure p_H, which are used as normalizers for spatial coordinates and for stresses, respectively.

The target computational domain was chosen as a cuboid of side lengths $4a_H \times 4a_H \times 2a_H$ meshed with $128\times128\times128$ grids. It should be noted that, according to the proposed method, the influence coefficients computation is performed in a domain 16 times larger in each tangential direction, consequently $16^2 \cdot 128^3$ different influence coefficients need to be computed. Nonetheless, each contact simulation was performed in less than ten minutes on a 4 core 3.2GHz CPU, whereas the memory utilization did not exceed 8 gigabytes of RAM. The value of the frequency response function at the origin in the frequency domain was computed numerically using the Matlab function "quad2d" with the default absolute and relative tolerances. No convergence issues were encountered during the simulations. In each point of the 3D mesh, the six stress tensor components were computed, as well as the von Mises equivalent stress, defined in relation to the stress tensor second invariant J_2:

$$\sigma_{VM} = \sqrt{3J_2} = \sqrt{\frac{1}{2}\left[(\sigma_{xx}-\sigma_{yy})^2+(\sigma_{yy}-\sigma_{zz})^2+(\sigma_{zz}-\sigma_{xx})^2+6(\sigma_{xy}^2+\sigma_{yz}^2+\sigma_{zx}^2)\right]}. \tag{11}$$

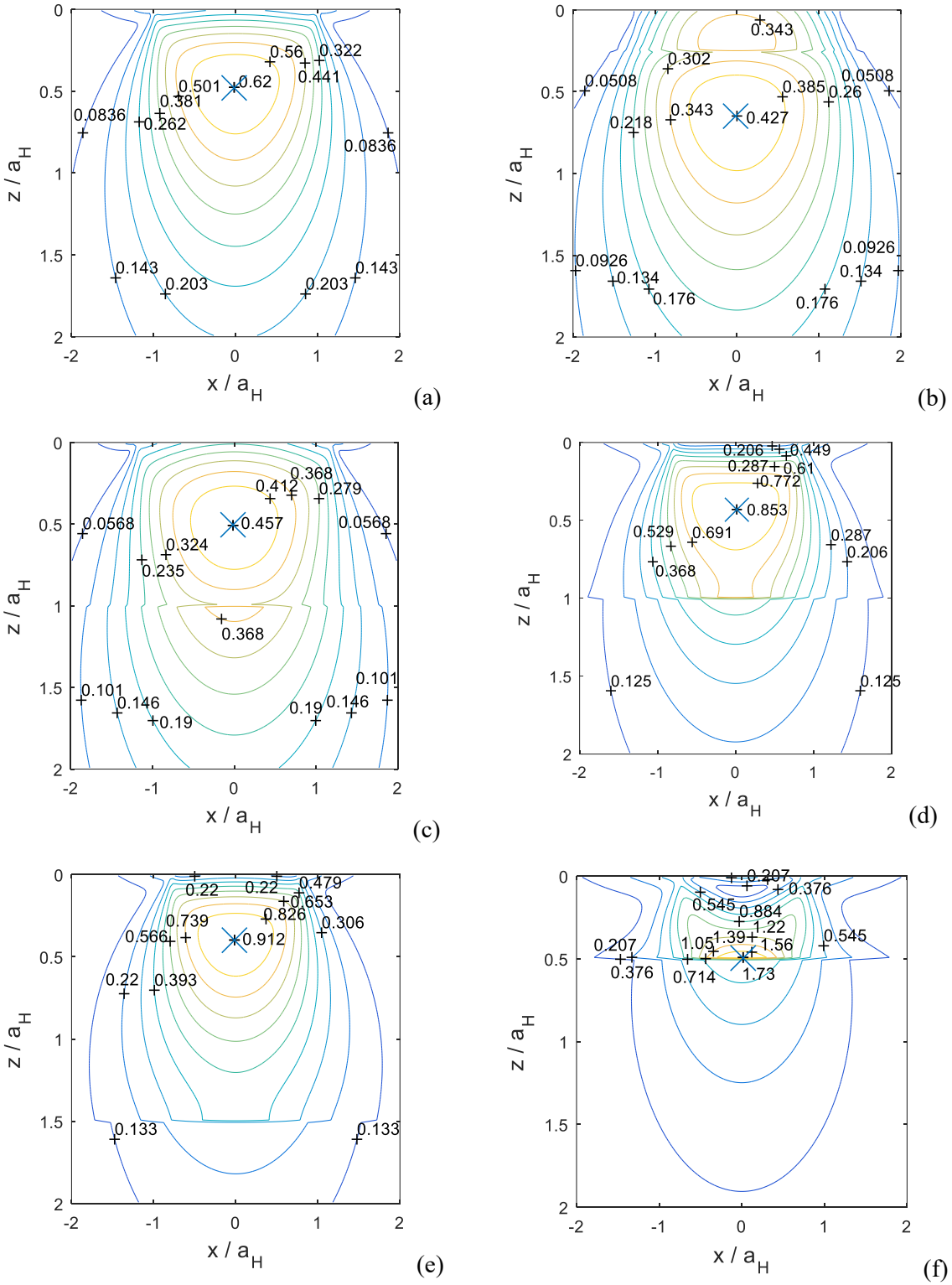

Figure 1. Iso-contours of dimensionless von Mises equivalent stress σ_{VM}/p_H : (a) $E_1/E_2=1$; (b) $E_1/E_2=1/4$, $h/a_H=1/4$; (c) $E_1/E_2=1/2$, $h/a_H=1$; (d) $E_1/E_2=2$, $h/a_H=1$; (e) $E_1/E_2=2$, $h/a_H=3/2$; (f) $E_1/E_2=4$, $h/a_H=1/2$. Location of the maximum is denoted by the symbol "X".

The latter parameter defines the yield surface and is used to predict plastic yield and/or crack nucleation inside the elastic medium, when its magnitude exceeds the yield strength of the elastic material. A set of numerical simulations was performed with varying dimensionless layer thickness h/a_H and varying coating elastic modulus. Typical results are presented in figure 1. The maximum intensity of von Mises equivalent stress σ_{VM}/p_H for each contact simulation, as well as its location, are presented in table 1. Results in figures 1(a), (c) and (d) match well contours plots presented in the literature [2,12] for the same contact scenarios.

Table 1. Influence of layer thickness and of the elastic modulus on the maximum equivalent stress

	$h/a_H = 1/4$	$h/a_H = 1/2$	$h/a_H = 1$	$h/a_H = 3/2$
$E_1/E_2 = 1/4$	0.427 (substrate)	0.3671 (substrate)	0.3346 (coating)	0.3073 (coating)
$E_1/E_2 = 1/2$	0.534 (substrate)	0.4815 (substrate)	0.4569 (coating)	0.4336 (coating)
$E_1/E_2 = 1$	0.6197	0.6197	0.6197	0.6197
$E_1/E_2 = 2$	0.6952 (interface)	0.9896 (interface)	0.8533 (coating)	0.9125 (coating)
$E_1/E_2 = 4$	1.069 (interface)	1.7298 (interface)	1.2328 (coating)	1.3922 (coating)

The numerical simulations predict that the maximum stress differs significantly from the homogenous case. More compliant coatings (i.e., smaller E_1/E_2) lead to lower maximum stresses, located in the substrate when the coating is thin, or in the coating otherwise. The maximum stresses appear to decrease slightly with the increase in the layer thickness. On the other hand, when the coating is stiffer than the substrate (i.e., $E_1/E_2 > 1$), there is an important increase in the maximum equivalent stress, which is located in the coating if the latter is thick, or near the interface when the coating is thin. Additional investigations may be needed for the optimal design of the coated system. In all cases, the iso-contours of the von Mises stress are discontinuous at the interface, and the gap increases with the dissimilarity in elastic properties between the coating and the substrate.

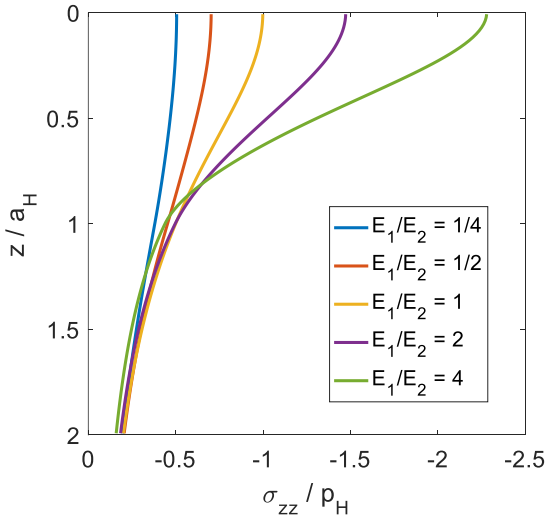

Figure 2. The σ_{zz} stress component on the z-axis, $h/a_H = 1$.

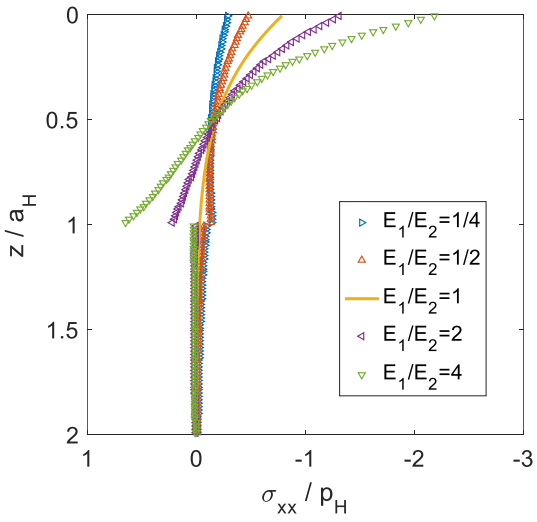

Figure 3. The σ_{xx} stress component on the z-axis, $h/a_H = 1$.

Figures 2 and 3 depict the stress components σ_{zz} and σ_{xx} on the contact axis. i.e. at $x = y = 0$, for the case $h/a_H = 1$. The figures suggests that, the stiffer the coating, the larger the maximum values of

both σ_{xx} and σ_{zz}. It should be noted that σ_{zz} is continuous across the interface (i.e., at $z/a_H = 1$), in agreement with the continuity condition (3), whereas σ_{xx} is discontinuous. Figure 3 also suggests that, for coatings stiffer than the substrate, σ_{xx} becomes tensile near the interface, whereas in the other cases it is always compressive. A tensile stress may favor the propagation of cracks orthogonal to the interface at the base of the layer. The changing sign of the σ_{xx} stress component suggests that the stiffer coating behaves as a thin plate subjected to a combination of membrane and bending stresses.

5. Conclusions

A semi-analytical simulation technique proposed in a companion paper is extended for stress analysis in the quasi-static contact of a rigid sphere pressed against a coated system consisting in a layer on top of an elastically dissimilar substrate. The method is based on closed-form expressions of the frequency response functions for stresses in a layered half-space derived in the literature by Fourier analysis.

The discrete sample of the frequency response function corresponding to the elementary cell centred in origin is calculated numerically as the mean value of the function over the latter cell. This computation releases the singularity in origin, as the frequency response functions are integrable everywhere. With this modification, the algorithm for the computation of convolution products in the frequency domain can also be used for stress analysis, in which absolute rather than relative values are required to predict plastic yielding and/or crack nucleation.

The computer program predictions match well existing results obtained by different methods. A preliminary study of the influence of layer thickness and of the dissimilarity in the elastic properties between the layer and the substrate is performed. It is found that the maximum intensity of the von Mises equivalent stress can vary significantly from the homogenous case when the layer is stiffer than the substrate. Moreover, when the coating is thin, it behaves like a plate subjected to bending, with tensile stresses arising at the base of the layer, which may favor crack propagation in the direction normal to the interface.

From a computational point of view, the proposed simulation technique is fast enough to tackle the design of coated systems involving real microtopography of contacting surfaces. A more in-depth study of the optimal coating parameters leading to improved contact resistance is proposed for future analysis.

Acknowledgement

This work was partially supported from the project “Integrated Center for Research, Development and Innovation in Advanced Materials, Nanotechnologies, and Distributed Systems for Fabrication and Control”, Contract No. 671/09.04.2015, Sectoral Operational Program for Increase of the Economic Competitiveness co-funded from the European Regional Development Fund.

6. References

[1] King R B and O’Sullivian T C 1987 *Int. J. Solids Struct.* **23** 581
[2] O’Sullivian T C and King R B 1988 *J. Tribol. – Trans. ASME* **110** 235
[3] Chiu Y P and Hartnett M J 1983 *ASME J. Lubr. Technol.* **105** 585
[4] Cole S J and Sayles R S 1992 *J. Tribol. – Trans. ASME* **114** 334
[5] Ju Y and Farris T N 1996 *J. Tribol. – Trans. ASME* **118** 320
[6] Nogi T and Kato T 1997 *J. Tribol. – Trans. ASME* **119** 493
[7] Ai X L and Sawamiphakdi K 1999 *J. Tribol. – Trans. ASME* **121** 639
[8] Polonsky I A and Keer L M 2000 *J. Tribol. – Trans. ASME* **122** 30
[9] Liu S B, Wang Q and Liu G 2000 Wear **243** 101
[10] Liu S B and Wang Q 2002 *J. Tribol. – Trans. ASME* **124** 36
[11] Wang Z J, Wang W-Z, Wang H, Zhu D and Hu Y-Z 2010 *J. Tribol. – Trans. ASME* **132** 021403
[12] Yu C, Wang Z and Wang Q J 2014 *Mech. Mater.* **76** 102

Appendix

The following notations are used: $\alpha=\sqrt{m^2+n^2}$, $\theta=e^{-2\alpha h}$, $\mu=G_1/G_2$, $\kappa=(\mu-1)/(\mu+3-4\nu_1)$, $\lambda=1-4(1-\nu_1)/[1+\mu(3-4\nu_2)]$, $R=-\alpha^{-2}/[1+(\lambda+\kappa+4\kappa\alpha^2h^2)\theta+\lambda\kappa\theta^2]$, where m and n are the coordinates in the frequency domain corresponding to x and y, respectively, and G_i and ν_i are the shear moduli and the Poisson's ratios for the layer ($i=1$) and for the substrate ($i=2$). The following coefficients are defined:

$$A^{(1)}=R\left\{-(1-2\nu_1)[1-(1-2\alpha h)\kappa\theta]+\frac{1}{2}(\kappa-\lambda-4\kappa\alpha^2h^2)\theta\right\};\ \bar{A}^{(2)}=\bar{C}^{(2)}=0; \tag{12}$$

$$\bar{A}^{(1)}=R\theta\left\{(1-2\nu_1)\kappa(1+2\alpha h-\lambda\theta)+\frac{1}{2}(\kappa-\lambda-4\kappa\alpha^2h^2)\right\}; \tag{13}$$

$$A^{(2)}=-\frac{1}{2}R\sqrt{\theta}\left\{(3-4\nu_2)(1-\lambda)[1-(1-2\alpha h)]\kappa\theta]+(\kappa-1)(1+2\alpha h-\lambda\theta)\right\}; \tag{14}$$

$$C^{(1)}=[1-(1-2\alpha h)]\kappa\theta]\alpha R;\ \bar{C}^{(1)}=(1+2\alpha h-\lambda\theta)\kappa\theta\alpha R;\ C^{(2)}=(1-\lambda)\sqrt{\theta}C^{(1)}. \tag{15}$$

The frequency response functions of the pressure-induced six stress tensor components can then be expressed in the frequency domain, with $i=1$ for the layer and $i=2$ for the substrate:

$$\tilde{\sigma}_{xx}(m,n,z_i)=-m^2(A^{(i)}e^{-\alpha z_i}+\bar{A}^{(i)}e^{\alpha z_i})+2\alpha\nu_i(C^{(i)}e^{-\alpha z_i}-\bar{C}^{(i)}e^{\alpha z_i})-z_im^2(C^{(i)}e^{-\alpha z_i}+\bar{C}^{(i)}e^{\alpha z_i}); \tag{16}$$

$$\tilde{\sigma}_{yy}(m,n,z_i)=\tilde{\sigma}_{yy}(n,m,z_i); \tag{17}$$

$$\tilde{\sigma}_{zz}(m,n,z_i)=\alpha^2(A^{(i)}e^{-\alpha z_i}+\bar{A}^{(i)}e^{\alpha z_i})+2\alpha(1-\nu_i)(C^{(i)}e^{-\alpha z_i}-\bar{C}^{(i)}e^{\alpha z_i})+z_i\alpha^2(C^{(i)}e^{-\alpha z_i}+\bar{C}^{(i)}e^{\alpha z_i}); \tag{18}$$

$$\tilde{\sigma}_{xy}(m,n,z_i)=-mn(A^{(i)}e^{-\alpha z_i}+\bar{A}^{(i)}e^{\alpha z_i})-z_imn(C^{(i)}e^{-\alpha z_i}+\bar{C}^{(i)}e^{\alpha z_i}); \tag{19}$$

$$\tilde{\sigma}_{yz}(m,n,z_i)=\tilde{\sigma}_{xz}(n,m,z_i); \tag{20}$$

$$\begin{aligned}\tilde{\sigma}_{zx}(m,n,z_i)=-\sqrt{-1}\big[&m\alpha(A^{(i)}e^{-\alpha z_i}-\bar{A}^{(i)}e^{\alpha z_i})+m(1-2\nu_i)(C^{(i)}e^{-\alpha z_i}+\bar{C}^{(i)}e^{\alpha z_i})\\&+z_im\alpha(C^{(i)}e^{-\alpha z_i}-\bar{C}^{(i)}e^{\alpha z_i})\big].\end{aligned} \tag{21}$$